INTERNATIONAL JOURNAL FOR NUMERICAL METHODS IN FLUIDS, VOL. 23, 953–983 (1996)

MODELLING OF RELEASE OF GAS FROM HIGH-PRESSURE PIPELINES

IVAR ØYVIND SAND

Chr. Michelsen Research AS, Department of Process and Safety, P.O. Box 3, N-5036 Fantoft, Bergen, Norway

KARL SJØEN AND JAN ROAR BAKKE

Statoil, Norway

SUMMARY

The problem investigated is the break of a high-pressure pipeline carrying natural single-phase gas which may condensate (retrograde) when the pressure drops. Single-phase non-ideal gas is assumed using a generalized equation of state. Taking advantage of the choked massflow condition, the break is split into a pipe flow problem and a dispersion flow problem, both solved using a finite difference control volume scheme.

The transient flow field from the pipeline break location is expanded analytically, using an approximation of the governing equations, until ambient pressure is reached and matched to the corresponding gas dispersion flow field using as subgrid model a jet box with a time-varying equivalent nozzle area as an internal boundary of the dispersion domain. The turbulence models used for the pipe and dispersion flow fields are an empirical model of Reichard and the k–ϵ model for buoyant flow respectively.

The pipe flow simulations indicate that the flow from the pipeline might include dispersed condensate which will affect quantitatively the mass flow rate from the pipeline and qualitatively the gas dispersion if the condensate rains out.

The transient dispersion simulation shows that an entrainment flow field develops and mixes supersaturated gas with ambient warmer air to an unsaturated mixture. Because of the inertia of the ambient air, it takes time to develop the entrainment flow field. As a consequence of this and the decay of the mass flow with time, the lower flammability limit of the gasair mixture reaches its most remote downstream position relatively early in the simulation (about 15 s) and withdraws closer to the break location.

KEY WORDS: transient pipeflow; non-ideal gas; subgrid modelling; transient dispersion

1. INTRODUCTION

The use of natural gas as an energy source and raw material in the petrochemical industry leads to transport of large quantities of gas. In many cases this transport is carried out by flowing the gas through pipelines.

The problem studied is the break of a long pipeline which carries wet natural gas under very high pressure. If the pipeline breaks, the escaping gas will mix with the ambient air to a mixture with flammability limits that depend on the mixture equivalence ratio (ratio between mass fractions of natural gas and oxygen compared with their stoichiometric ratio). The gas will not burn if the mixture becomes too rich or too lean. To predict the consequences of a pipeline break, it is therefore necessary to know the temperal and spatial variations in the gas mixture concentration. This requires

CCC 0271–2091/96/090953–31

Received August 1992
Revised November 1995

detailed knowledge about the topology of the release area, the mass and momentum fluxes of the gas and ambient air and their states.

To facilitate the problem, we assume that the pipeline is subjected to a full guillotine break at the end where the pressure is lowest. Basically this means that we study a case where the geometry of the break opening does not have too much influence on the mass and momentum flows. We also avoid handling the counterflowing field of natural gas which would occur if the pipeline break were not located at an end of the pipeline. The problem is simplified further by assuming that the release area is limited by a plane with friction (representing the ground), a vertical symmetry plane though the centreline of the pipe and three boundaries where the flow is free to flow into or out of the computational domain depending on how the flow field develops.

At the break instance the temperature is assumed to be the same inside and outside the pipeline. We also assume that the air outside the pipeline is at rest initially. The numerical computations are based on the assumption that the compressible fluid is always in the gas phase, which means that the gas becomes supersaturated if its dynamic state corresponds to a two-phase equilibrium state. How the mass flow depends on liquid condensation is discussed briefly in Section 6.2.

The numerical procedure established is used for computation of the non-ideal highly transient gas flow from a reservoir under high pressure (a long pipeline). The main problem is split into two, where the first problem is transient flow in a pipeline neglecting downstream effects because of choking. The second problem is transient dispersion of gas downstream of the pipeline break location where the flow field is driven by the momentum flux from the pipeline break.

To include real gas effects in our computations, we use the Benedict, Web, Rubin and Starling generalized equation of state for the gas flow both inside and outside the pipeline. The governing equations for the flow and concentration fields in the pipeline are assumed to be one-dimensional. However, when the bulk flow equations are derived, the radial variation is taken into account using an empirical velocity profile for fully developed turbulent axisymmetrical pipe flow and an empirical turbulence viscosity given by Reichardt[1]; see Section 2.1. Within the pipeline, heat generation caused by viscous dissipation is computed using a two-layer wall function model for the momentum boundary layer. The heat flux from the environment to the pipe flow is modelled using an empirical relation for turbulent pipe flow by Petukov.[2]

The gas dispersion problem is solved assuming that the pipeline break location is an internal boundary of the computational domain; see Section 3.4. An approximation of the governing conservation equations in integral form[3] is improved and used to expand analytically the one-dimensional choked flow field from the pipeline break to that of a supersonic turbulent jet and to match it to the three-dimensional gas dispersion flow field; see Section 3.4.

When the ambient air mixes with the wet gas injected from the turbulent supersonic jet, we use the two-stream mixing process[4] to find the molar fractions of the gas composition; see Section 3.3. We approximate the effect of the ground on the flow field by a horizontal plane with friction. The viscous shear forces from the plane acting on the flow field are computed using a two-layer wall function procedure for the momentum boundary layer and for the production and dissipation rate of turbulent kinetic energy.[5]

When an isothermal boundary condition is used at the ground, an analogous two-layer wall function procedure is used for the thermal boundary layer to calculate the heat flux from the ground. Buoyancy is modelled as well as its effect on turbulence production and destruction.[6]

The governing equations for the pipe and dispersion flow problems are presented in Sections 2 and 3 respectively. The numerical solution procedure is given briefly in Section 4. In Section 6 we discuss the pipeline break problem, present our results, give some comments on the numerical accuracy and give a comparison of the transient simulations with small-scale data from an underexpanded steady jet for varying reservoir pressure. Conclusions are presented in Section 7.

2. GOVERNING EQUATIONS FOR PIPE FLOW PROBLEM

We assume that the flow and concentration fields are axisymmetrical, fully turbulent developed and can be described by mass-weighted time-averaged conservation equations for mass, momentum and specific enthalpy.[7] The problem is also governed by a turbulence model, an equation of state and boundary and initial conditions.

2.1. Turbulence model and conservation equations for bulk flow

The conservation equation for mass is given by

$$\frac{\partial \rho}{\partial t} + \frac{\partial}{\partial x}(\rho V) = 0, \tag{1}$$

where the bulk velocity is defined by

$$V = \frac{1}{A}\int_A U \, \mathrm{d}A \tag{2}$$

and U is the mass-weighted time-averaged velocity.

To find a bulk form of the conservation equation for momentum, we start with its mass-weighted time-averaged axisymmetrical form and approximate the turbulent viscosity using an empirical relation given by Reichardt,[1]

$$\mu_t = \tfrac{1}{6}\rho\kappa(r_0 - r)(\tau_w/\rho)^{\frac{1}{2}}(1 + r/r_0)[1 + 2(r/r_0)^2], \tag{3}$$

where κ is the von Karman constant, and r_0 is half the pipe diameter and τ_w is the wall shear, which is related to the density and the bulk velocity by the definition of the drag coefficient

$$C_f = 2\,\tau_w/(\rho V^2). \tag{4}$$

We assume that the pipe wall is smooth and use the drag coefficient recommended by Petukov,[2]

$$C_f = 2/(2{\cdot}236 \ln Re - 4{\cdot}639)^2, \tag{5}$$

where Re is the Reynolds number for the bulk flow. To include the radial dependence in the velocity, we use a measured velocity profile[8]

$$U = U_c[(r_0 - r)/r_0]^{1/7}, \tag{6}$$

where U_c is the centreline velocity.

We substitute these relations into the conservation equation for momentum and integrate with respect to r over the axisymmetrical cross-section. It follows that the bulk form of the momentum equation is given by

$$\frac{\partial}{\partial t}(\rho V) + \frac{\partial}{\partial x}(\rho V^2) = -\frac{\partial p}{\partial x} + \frac{4}{3}\frac{\partial^2}{\partial x^2}(\mu^*_{\mathrm{eff}} V) - \frac{4}{D}\rho C_f V \| V \|, \tag{7}$$

where the new effective viscosity is given by

$$\mu^*_{\mathrm{eff}} = 0{\cdot}146\rho\kappa r_0 (C_f/2)^{\frac{1}{2}} \| V \|. \tag{8}$$

We have neglected $(\partial/\partial x)(\rho V^2)/49$, which has its origin in the variation in the kinetic energy with the pipe radius,[9] compared with the error we have made by using the velocity profile given by (6). The neglected term decreases as the Reynolds number increases, because the turbulent velocity profile develops a box-formed shape. We have also neglected $(1/A)\int_A(\frac{2}{3}\rho k)\,dA$ compared with $\frac{4}{3}(\partial^2/\partial x^2)(\mu^*_{\text{eff}}V)$, because it can be shown, on the basis of experiments carried out by Laufer,[10] that the turbulent kinetic energy $k \sim C_f$. From (8) it follows that $\mu^*_{\text{eff}} \sim C_f^{1/2}$. For our Reynolds number range (10^4–10^7), $C_f^{1/2}$ is one order of magnitude greater than C_f; see the friction coefficient of Moody in Reference 8.

The specific enthalpy does not have the same r-dependence as U, since heat is generated in the shear layer close to the pipe wall. However, since the source terms which are most important during high-velocity and transient flow are independent of h, we simplify the equation by assuming that h has the same r-dependence as U and get the conservation equation

$$\frac{\partial}{\partial t}(\rho h) + \frac{\partial}{\partial x}(\rho V h) = \frac{\partial}{\partial x}\left(\frac{\mu^*_{\text{eff}}}{\sigma_h}\frac{\partial h}{\partial x}\right) + \frac{\mathrm{D}p}{\mathrm{D}t} + \frac{1}{A}\int_A \Phi\,dA + \dot{Q}, \tag{9}$$

where Φ is the dissipation term, given in cylindrical co-ordinates in Reference 11, and σ_h is the turbulent Schmidt number; see Table I.

We assume that the flow field is axisymmetrical and has a negligible gradient in the flow direction. The flow field is divided in an inner and an outer domain where the velocity field in non-dimensional variables is given by

$$u^+ = \begin{cases} y^+ & \text{for } y^+ \leqslant y_v^+, \\ 8{\cdot}6(y^+)^{1/7} & \text{for } y^+ > y_v^+, \end{cases} \tag{10}$$

where $u^+ = u/(\tau_w/\rho)^{1/2}, y^+ = (r_0 - r)(\tau_w/\rho)^{1/2}/\nu, y_v^+$ is the thickness of the inner domain, τ_w is given by (2), (4) and (6) and C_f is given by (5). In the numerical simulations we use $y_v^+ = 11$; see Reference 8.

It follows that the average dissipation per unit volume is

$$\bar{\Phi} \approx \frac{\tau_w\,\nu}{r_0^2}\left\{\frac{(8{\cdot}6)^2}{35}(y_v^+)^{2/7}\left[\frac{2r_0^+}{y_v^+} + 5 - 7\left(\frac{r_0^+}{y_v^+}\right)^{2/7}\right] + (y_v^+)^2\left(\frac{2r_0^+}{y_v^+} - 1\right)\right\}. \tag{11}$$

The heat flux from the experiment to the pipe flow was modelled using an empirical relation for turbulent pipe flow by Petukov,[2]

$$\dot{Q} = (T_w - T)\,\rho c_p \|V\|(C_f/2)[1{\cdot}07 + 12{\cdot}7(P_r^{2/3} - 1)(C_f/2)^{1/2}]^{-1}, \tag{12}$$

where T_w, T, c_p and P_r are the wall temperature, the bulk temperature, the specific heat capacity at constant pressure and the Prandtl number respectively. For a Prandtl number greater than or equal to 0·7, formula (12), originally developed for constant heat flux, is, within the accuracy of the formula, identical with that of constant wall temperature.[8]

Table I. Constants appearing in governing equations

C_1	C_2	C_3	$C_{\mu\infty}$	σ_ε	σ_k	σ_h	$\sigma_{f_{\text{mix}}}$	Pr_t
1·44	1·92	0·8	0·09	1·3	1·0	0·7	0·7	0·9

2.2. *Generalized equation of state*

To handle accurately a real gas composition, we use the generalized equation of state.

$$p = \rho RT + F, \tag{13}$$

where p, ρ, R, T and F are the pressure, the density, the specific gas constant, the absolute temperature and the departure from ideal gas behaviour respectively.

The specific gas constant is given by

$$R = \mathscr{R} \Big/ \left(\sum_{i=1}^{N} W_i X_i \right), \tag{14}$$

where $\mathscr{R}$, W_i and X_i are the universal gas constant, the molar weight and the molar fraction of the ith gas component respectively and N is the number of gas components in the mixture. We use the Benedict, Webb, Rubin and Starling generalized equation of state (BWRSGES)

$$\begin{aligned} F =& (B_0 \mathscr{R}T - A_0 - C_0/T^2 + D_0/T^3 - E_0/T^4)\hat{\rho}^2 + (b\mathscr{R}T - a - d/T)\hat{\rho}^3 \\ &+ \alpha(a + d/T)\hat{\rho}^6 + c(\hat{\rho}^3/T^2)(1 + \gamma\hat{\rho}^2)\exp(-\gamma\hat{\rho}^2), \end{aligned} \tag{15}$$

where $\hat{\rho}$ is the molar density defined by $\hat{\rho} = \rho R/\mathscr{R}$. The 11 parameters used in (15) are given by mixing rules for pure gas equation parameters, molar fractions and binary interaction coefficients. Equation parameters and binary interaction coefficients are determined by curve fitting to experimental data.[12]

2.3. *Boundary conditions for pipe flow problem*

The release of gas from a long pipeline under decompression can be classified on the basis of the temporal variation in the mass flow. The following three flow regimes are easily distinguishable: the initial flow regime, where the inertial forces are stronger than the viscous forces, the wave-dominated flow regime, where the pressure at the open end approaches the ambient pressure, and the quasi-steady flow regime, where the gas flow in the pipeline is affected everywhere by the gas release. These flow regimes last for the order of seconds, minutes and hours respectively.[13]

For a short period of the initial flow regime, before the flow becomes choked, we compute the velocity and density at the break location by solving simultaneously the continuity and the Euler momentum equations by an implicit numerical procedure.[14]

For choked flow and non-ideal gas one can show, using the isentropic index $K = (\rho/p)(\partial p/\partial\rho)_T\gamma$ instead of γ,[15] the continuity equation and the Euler momentum equation, that the mass flux passing a reference point (subscript 'r') upstream of the throat (subscript 't') is given by

$$\dot{m} = C_D A_r \rho_r \left\{ \frac{2K}{K-1} \frac{p_r}{\rho_r} \left(1 - r^{1-1/K}\right) \Big/ \left[\left(\frac{A_r}{A_t}\right)^2 \left(\frac{1}{r}\right)^{2/K} - 1 \right] \right\}^{1/2}, \tag{16}$$

where C_D is a discharge coefficient, γ is the specific heat capacity ratio (c_p/c_v) and $r = p_t/p_r$.[16] It should be noted that for a pressure a few bars over the atmospheric pressure, K is practically identical with γ also for a non-ideal gas.

To determine r such that $\dot{m}$ has a maximum, we differentiate the last factor on the right side of (16) with respect to r. It follows that extreme values occur for

$$r^{1-1/K} - \frac{K}{K+1}\left(\frac{A_t}{A_r}\right)^2 r^{1+1/K} - \frac{2}{K+1} = 0. \tag{17}$$

We solve this transcendental equation using the Newton–Raphson method. The algorithm is given by

$$r_{n+1} = r_n - F(r_n)/F'(r_n), \tag{18}$$

where F is equal to the left side of (17). As a start guess for the iteration procedure we use the solution of (17) neglecting the second term, which is

$$r_{ci} = \left(\frac{2}{K+1}\right)^{K/(K-1)}. \tag{19}$$

The choked boundary condition is then invoked for $p_t/r_r < r_c$, where r_c is the solution of (17).

The outflow boundary conditions for choked flow are

$$V_t = C_D c_s \quad \text{at } x = L, \tag{20}$$

$$\rho_t = \rho_r r_c^{1/K} \quad \text{at } x = L, \tag{21}$$

$$p_t = r_c p_r \quad \text{at } x = L, \tag{22}$$

where L is the length of the pipeline and c_s is the velocity of sound. The scalars used in the choked flow boundary conditions are computed from relations derived on the basis of the BWRSGES; see Sections 2.2 and 2.4–2.6.

2.4. *Computational procedure for equilibrium density*

To compute the equilibrium density when the pressure, temperature and mixture molar fractions are known, we use the Navier–Raphson method to solve

$$p - \rho RT - F = 0. \tag{23}$$

Since we only consider variation with respect to ρ, we get the algorithm

$$\rho_{n+1} = \rho_n - \Psi(\rho_n)/\Psi'(\rho_n), \tag{24}$$

where Ψ is given by the left side of (23). As a start guess for the algorithm we use initially the equilibrium density given by $\rho = p/(RT)$ and for any following time step the dynamic density from the preceding time step. For the corresponding temperature we start with the initial temperature and use the temperature from the preceding time step for any following time step.

2.5. *Computational procedure for temperature field*

To compute the temperature when the dynamic density and dynamic specific enthalpy are known, we use the Newton–Raphson method to solve

$$h - h_d = 0, \tag{25}$$

where h_d is the dynamic specific enthalpy which satisfies (9) and h is the equilibrium specific enthalpy of the fluid mixture which is defined on the basis of the BWRSGES, given by

$$\begin{aligned} h = {} & h_0 + (B_0 \mathscr{R}T - 2A_0 - 4C_0/T^2 + 5D_0/T^3 - 6E_0/T^4)\hat{\rho} \\ & + \tfrac{1}{2}(2b\mathscr{R}T - 3a - 4d/T)\hat{\rho}^2 + (\alpha/5)(6a + 7d/T)\hat{\rho}^5 \\ & + (c/\gamma T^2)\{3[1 - \exp(-\gamma\hat{\rho}^2)] - (\gamma\hat{\rho}^2/2)\exp(-\gamma\hat{\rho}^2) + \gamma^2\hat{\rho}^4 \exp(-\gamma\hat{\rho}^2)\}. \end{aligned} \tag{26}$$

Table II. Molar fractions for wet gas composition

Component	X_{lm}
C_1	0·7599
C_2	0·1119
C_3	0·0738
$i-C_4$	0·0084
$n-C_4$	0·0200
$i-C_5$	0·0061
C_{6+}	0·0000
N_2	0·0060
CO_2	0·0078

Here h_0 is the ideal part of the equilibrium enthalpy and is a function of molar fractions and temperature. Since we consider only variation with respect to T, we get

$$T_{n+1} = T_n - \Psi(T_n)/\Psi'(T_n), \tag{27}$$

where Ψ is the left side of (25). As a start guess for the algorithm we use the temperature from the preceding time step. The dynamic density used when computing Ψ is from the simultaneous time step.

2.6. *Velocity of sound in a non-ideal gas*

For a non-ideal gas mixture the velocity of sound is a function of temperature and density. The following thermodynamic relations[17] are used to compute c_s:

$$c_s^2 \equiv \left(\frac{\partial p}{\partial \rho}\right)_S = \left(\frac{c_p}{c_v}\right)\left(\frac{\partial p}{\partial \rho}\right)_T, \tag{28}$$

$$c_p = c_v + \frac{T}{\rho^2}\left(\frac{\partial p}{\partial T}\right)_\rho^2 \Big/ \left(\frac{\partial p}{\partial \rho}\right)_T. \tag{29}$$

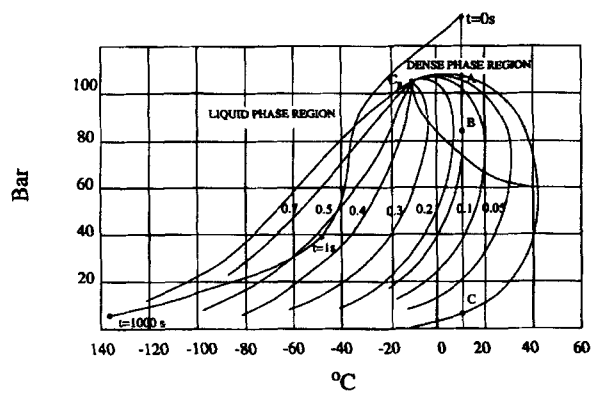

Figure 1. Wet gas phase envelope, computed state of wet gas at pipe exit as a function of time, and upper bound for effect of including heat of condensation

To relate c_v to the equilibrium enthalpy, we use the definition of enthalpy. It follows that

$$c_v = \left(\frac{\partial h}{\partial T}\right)_\rho - \frac{1}{\rho}\left(\frac{\partial p}{\partial T}\right)_\rho. \tag{30}$$

We compute the remaining partial derivatives of p and h using (13)–(15) and (26). The accuracy of those relations has been tested by a series of static computations using pure nitrogen and the wet gas mixture given in Table II. The results are given in Tables IV and V respectively (see Section 6). For pure nitrogen all tests converge. When we use the wet gas mixture, all tests converge except those which are carried out for an absolute temperature of 200 K with a pressure in the range 50–200 bar. However, in these states the gas is either in the liquid phase region or close to it; see Figure 1.

3. GOVERNING EQUATIONS FOR DISPERSION PROBLEM

Transient and stationary turbulent flows may be described by conservation equations for the variation in mass-weighted time-mean quantities.[7] Essentially these conservation equations are assumed to have the same form as the time-averaged conservation equations describing incompressible flow. The problem is also governed by an equation of state, a turbulence model and boundary and initial conditions.

3.1. Conservation equations and turbulence model

Conservation of mass is given by

$$\frac{\partial \rho}{\partial t} + \frac{\partial}{\partial x_i}(\rho U_i) = 0. \tag{31}$$

Conservation of momentum is given by

$$\frac{\partial}{\partial t}(\rho U_i) + \frac{\partial}{\partial x_j}(\rho U_j U_i) = -\frac{\partial p}{\partial x_i} + \frac{\partial}{\partial x_j}(\sigma_{ij}) + F_i, \tag{32}$$

where

$$\sigma_{ij} = \mu_{\text{eff}}\left(\frac{\partial U_i}{\partial x_j} + \frac{\partial U_j}{\partial x_i}\right) - \frac{2}{3}\delta_{ij}\left(\rho k + \mu_{\text{eff}}\frac{\partial U_k}{\partial x_k}\right), \tag{33}$$

$F_3 = -g(\rho - \rho_0)$, $F_i = 0$ for $i \neq 3$, ρ_0 is the initial density and g is the gravitational acceleration.

The effective viscosity is defined by

$$\mu_{\text{eff}} = \mu + \mu_t, \tag{34}$$

where μ and μ_t are the laminar and the turbulent viscosity respectively.

The turbulence model used is the k–ε model of Launder and Spalding.[18] In this model the turbulent viscosity is related to the turbulent kinetic energy k and its rate of dissipation ε by

$$\mu_t = C_{\mu\infty}\rho k^2/\varepsilon, \tag{35}$$

where k and ε are governed by conservation equations.

Conservation of turbulent kinetic energy is given by

$$\frac{\partial}{\partial t}(\rho k) + \frac{\partial}{\partial x_j}(\rho U_j k) = \frac{\partial}{\partial x_j}\left(\frac{\mu_{\text{eff}}}{\sigma_k}\frac{\partial k}{\partial x_j}\right) + P_k + G - \rho\varepsilon, \tag{36}$$

where the production rates of turbulent kinetic energy from stress and buoyancy are defined by

$$P_k = \sigma_{ij}\frac{\partial U_i}{\partial x_j} \quad \text{and} \quad G = \frac{\mu_t g_i}{\rho Pr_t}\frac{\partial \rho}{\partial x_i}$$

respectively, $g_3 = g$, $g_i = 0$ for $i \neq 3$ and Pr_t is the turbulent Prandtl number.

Conservation of dissipation rate of turbulent kinetic energy is given by

$$\frac{\partial}{\partial t}(\rho\varepsilon) + \frac{\partial}{\partial x_j}(\rho U_j \varepsilon) = \frac{\partial}{\partial x_j}\left(\frac{\mu_{\text{eff}}}{\sigma_\varepsilon}\frac{\partial \varepsilon}{\partial x_j}\right) + [C_1(P_k + G)(1 + C_3 R_f) - C_2\rho\varepsilon]\frac{\varepsilon}{k}, \tag{37}$$

where

$$R_f = -\frac{(U_1^2 + U_2^2)^{1/2}}{(U_1^2 + U_2^2 + U_3^2)^{1/2}}\frac{G}{P_k + G} \tag{38}$$

is a modified Richardson number which is zero for vertical flow.[6]

Conservation of specific enthalpy is given by

$$\frac{\partial}{\partial t}(\rho h) + \frac{\partial}{\partial x_j}(\rho U_j h) = \frac{\partial}{\partial x_j}\left(\frac{\mu_{\text{eff}}}{\sigma_h}\frac{\partial h}{\partial x_j}\right) + \frac{\mathrm{D}p}{\mathrm{D}t} + \Phi + \dot{Q}, \tag{39}$$

where Φ is the time-averaged viscous dissipation modelled as

$$\Phi = \mu\left[\left(\frac{\partial U_i}{\partial x_j} + \frac{\partial U_j}{\partial x_i}\right)^2 - \frac{2}{3}\left(\frac{\partial U_k}{\partial x_k}\right)\right] + \rho\varepsilon \tag{40}$$

and $\dot{Q}$ is the heat flux from the ground modelled by a two-layer wall function procedure for the thermal boundary layer; see Section 3.2.

Conservation of mixture fraction is given by

$$\frac{\partial}{\partial t}(\rho f_{\text{mix}}) + \frac{\partial}{\partial x_j}(\rho U_j f_{\text{mix}}) = \frac{\partial}{\partial x_j}\left(\frac{\mu_{\text{eff}}}{\sigma_{f_{\text{mix}}}}\frac{\partial f_{\text{mix}}}{\partial x_j}\right), \tag{41}$$

where the mixture fraction f_{mix} is defined in Section 3.3.

The constants appearing in the governing equations are given in Table I. To handle accurately a real gas composition, we use the BWRSGES; see (13)–(15) and (26).

3.2. Near-wall regions

Wall functions are used to account for the momentum boundary layer in the near-wall region of the flow field without resolving it numerically. This is achieved by modifying the source terms in the governing equations for momentum using a two-layer model for the wall shear.[5] This model also modifies the source terms in the conservation equations for turbulent energy and its rate of dissipation.

An analogous two-layer wall function procedure is implemented for the thermal boundary layer to calculate the heat flux from the wall when an isothermal boundary condition is used.[19]

3.3. Two-stream mixing process

To find the molar fraction distribution needed in the BWRSGES, we consider a two-stream mixing problem.[4] The fluid B mixes with the ambient fluid A to form the mixture fluid M. We assume that all

gas components in the fluids A and B have the same diffusivity and that there is no chemical reaction. Then the molar fraction of the jth gas component of the mixing stream is given by

$$X_{jM} = [f_{mix} W_A X_{jB} + (1 - f_{mix}) W_B X_{jA}]/[f_{mix} W_A + (1 - f_{mix}) W_B], \tag{42}$$

where the mixture fraction is defined as

$$f_{mix} = (m_{jM} - m_{jA})/(m_{jB} - m_{jA}), \tag{43}$$

W_A and W_B are the molar weights of the fluids A and B, respectively and m_{jM}, m_{jA} and m_{jB} are the mass fractions of the mixing stream and the fluids A and B respectively.

3.4. Matching procedure for pipe flow and dispersion problem

The choice of boundary conditions at the interface between the one-dimensional pipe flow and the three-dimensional dispersion flow depends on the flow regime. With the exception of a very short time interval (less than 1 s compared with hours) the flow at the pipeline break location is choked and thus pressure disturbances occurring downstream of the break location cannot propagate upstream of it. Therefore only secondary effects from the flow field downstream of the pipeline break location will influence the flow field inside the pipeline.

Consequently the one-dimensional pipe flow problem can be decoupled from the dispersion problem. The results from the numerical simulation of the pipe flow problem are stored on a file and used as time-varying boundary conditions at an internal boundary of the three-dimensional dispersion domain.

To avoid resolving the high pressure gradient at the pipeline break location within the three-dimensional domain, the underexpanded flow is modelled on subgrid level using simplified conservation equations in integral form to compute approximately the equivalent nozzle area corresponding to the exit area of the shock structure of nozzle form observed on schlieren photographs of underexpanded jets;[17] see Figure 2.

The nozzle area and the expanded variables are used at the entrance of a supersonic turbulent jet. The procedure follows mainly Reference 3. However, the reference condition in our work is modified to account for high velocities, while Birch *et al.*[3] use the stagnation reservoir condition. We also include the enthalpy equation in the procedure and thereby make the assumption of recovered temperature at the equivalent turbulent jet origin unnecessary.

To review the procedure, we consider a control volume. The pipeline break is chosen to be located at the entrance of this control volume, subscript 1. The control volume represents the equivalent nozzle and its exit corresponds to the origin of our turbulent jet, subscript 2; see Figure 2.

We assume negligible body forces, entrainment and viscous forces. We also assume that the exit pressure p_2 is equal to the ambient pressure p_a and that this after expansion is quasi-steady. From the ideal equation of state and the conservation equations for mass, momentum and specific enthalpy we get

$$U_2 = U_1 + (p_1 - p_a)/(\rho_1 U_1), \tag{44}$$

$$h_2 = h_1 + 0{\cdot}5(U_1^2 - U_2^2), \tag{45}$$

$$T_2 = T_1 + 0{\cdot}5(U_1^2 - U_2^2)/c_p, \tag{46}$$

$$\rho_2 = p_a/(RT_2), \tag{47}$$

$$A_2 = A_1 \rho_1 U_1/(\rho_2 U_2), \tag{48}$$

where A_2 is the exit area of the equivalent nozzle.

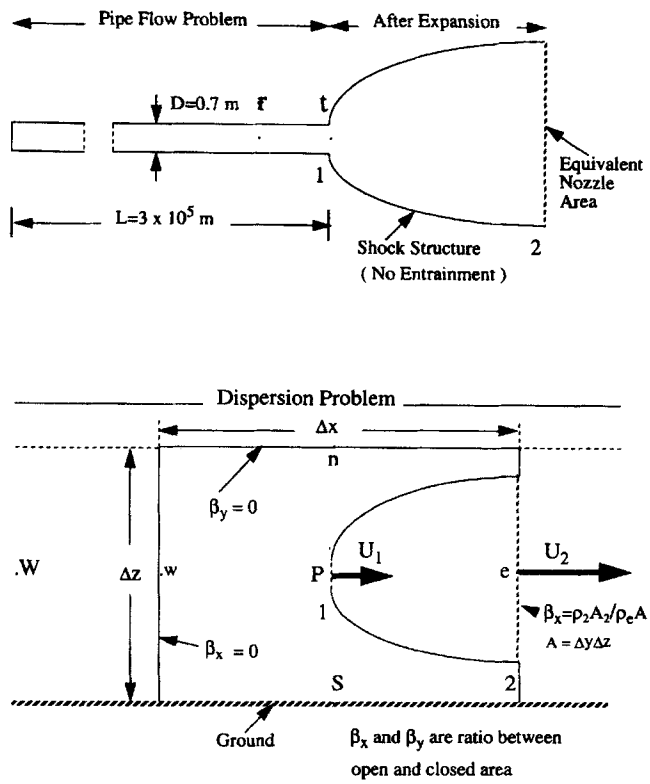

Figure 2. Illustration of physical problem with corresponding subgrid models

We can also derive (44) from jump conditions for the density and velocity assuming $A_1 \approx A_2$ during the initial shock. However, (44) is singular and is modified in the following way to handle the start from rest:

$$U_2 = U_1[1 + (p_1 - p_a)/(\rho_1 U_T^2)], \tag{49}$$

where

$$U_T = \begin{cases} C_D c_s & \text{for } U_1 \leqslant C_D c_s, \\ U_1 & \text{for } U_1 > C_D c_s. \end{cases} \tag{50}$$

The effect of this modification is that supersonic speed at the equivalent jet origin will be reached governed by the boundary condition procedure used for the pipe flow problem and not by the singular nature of (44). See Section 2.3, where in the initial phase we take into account the time-dependent terms in the conservation equations for mass and momentum.

3.5. *Matching of turbulence models*

We assume that the expansion of the flow field to ambient pressure is not affected by the viscosity. It follows that $k_2 = k_1$ and $\varepsilon_2 = \varepsilon_1$. The turbulence viscosity used in the pipe flow problem is given empirically by Reichardt.[1] Using both the k–l and the k–ε theory,[20] we get

$$k_2 = \mu_{t1}^2/(l_{m1} C_{\mu\infty}^{1/4} \rho_1)^2, \tag{51}$$

$$\varepsilon_2 = (\mu_{t1}/\rho_1)^3/l_{m1}^4, \tag{52}$$

where l_m is the mixing length, which for the pipe flow problem is given by Nikuradse's formula,[20] $C_{\mu\infty}$ is a turbulence coefficient; see Table I.

3.6. *Boundary conditions for dispersion problem*

We assume that the external boundaries are so open that choking will not occur. It follows for both inflow and outflow that

$$U_t = C_D \left\{ \frac{2c_s^2}{\gamma - 1} \left[1 - (p_t/p_r)^{1-1/\gamma} \right] \right\}^{1/2}, \tag{53}$$

$$\rho_t = \rho_r (p_t/p_r)^{1/\gamma}, \tag{54}$$

where the reference point (subscript 'r') is always located such that $p_t/p_r, \leqslant 1$.

For the other scalar variables we use the zero-gradient condition for both inflow and outflow,

$$\nabla\phi = 0 \quad \text{for } \phi = p, h, k, \varepsilon \text{ and } f_{mix}, \tag{55}$$

where ϕ at the boundary is equal to its nearest internal value and its initial value for outflow and inflow respectively. However, the pressure at the boundary is always set equal to its nearest internal value. This is done to assure that the pressure is determined by the time variation in the momentum flux from the supersonic turbulent jet, which is the driving force within the domain. The boundary conditions at the jet entrance are covered under the matching procedure (see Sections 3.4 and 3.5), with exception of the mixture fraction. To express that rich gas flows from the jet box into the domain, we set

$$f_{mix} = 1 \quad \text{within the jet box.} \tag{56}$$

4. SOLUTION PROCEDURE FOR GOVERNING EQUATIONS

The conservation and transport equations for the flow inside and outside the pipeline can be written in the form

$$\frac{\partial}{\partial t}(\rho\phi) + \frac{\partial}{\partial x_j}(\rho U_j \phi) = \frac{\partial}{\partial x_j}\left(\Gamma_\phi \frac{\partial \phi}{\partial x_j} \right) + S_\phi. \tag{57}$$

To solve these equations, we use a finite control volume method.[21] The calculation domain is divided into a discrete number of control volumes. Scalar properties are stored at the centre of each control volume, while each of the velocity components is located on a staggered grid coinciding with the control volume surface normal to its direction. Equations of the general form (57) are integrated over the control volumes using interpolation formulaes for the variation in ϕ between the grid points. Upwind differencing and a fully implicit formulation are used. The results is a set of algebraic

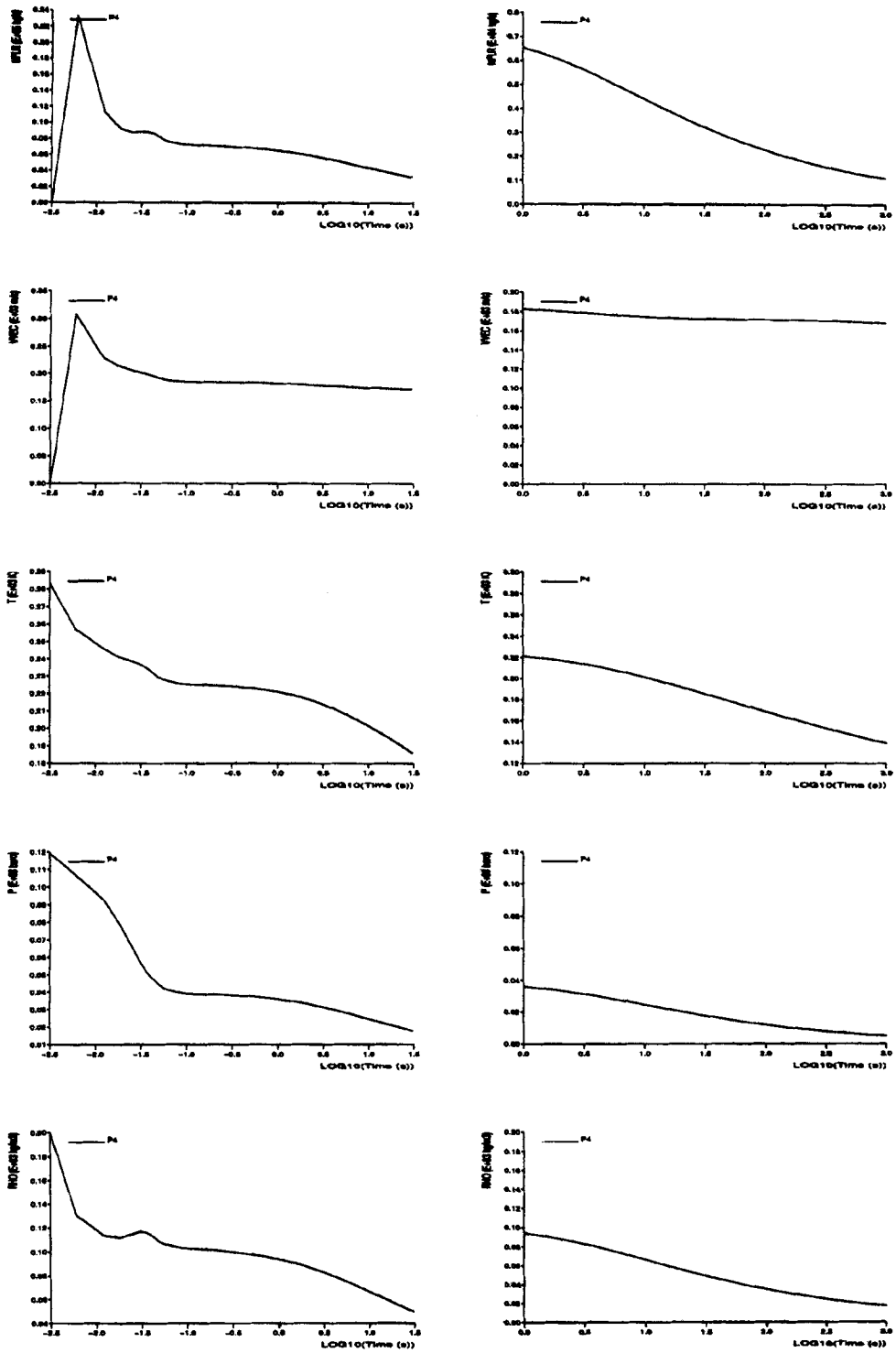

Figure 3. Flow rate, bulk velocity, temperature, pressure and density at end of pipeline (break location)

equations, where each equation connects the value of a scalar variable ϕ_P at a point P to its neighbour values ϕ_k.

The algebraic equations have the form

$$A_{P_\phi}\phi_P = \sum_{k=1}^{N} A_{k_\phi}\phi_k + S_{P_\phi}, \tag{58}$$

where $N = 6$ for the dispersion problem and $N = 2$ for the pipe flow problem. These algebraic equations are solved together with proper boundary and initial conditions by a tridiagonal matrix solver for all grid points within the computational domain. The velocity components computed within each time step are used as a first guess at the velocity field. The final values of the velocity components, the density and the pressure field are calculated using a variational procedure known as the SIMPLE method,[22] extended to account for compressibility. The conceptual idea behind this method is given by Chorin.[23] For details concerning the extension to compressibility, see Reference 24.

4.1. Use of a generalized equation of state

In our computational procedure we use the BWRSGES as the basis for finding the equilibrium density and equilibrium specific enthalpy, the velocity of sound, the specific heat capacity at constant pressure and the heat capacity ratio γ. The equilibrium density is used when we solve an approximate momentum equation to get an estimate of the velocity field. The estimated velocity field, the equilibrium density and the velocity of sound are used to compute coefficients needed in the pressure correction equation, which together with a variational procedure determines the pressure field, the dynamic density and the velocity field. The equilibrium and dynamic specific enthalpies are used to determine the temperature field. γ is used in the inflow and outflow boundary conditions; see Section 2.3.

5. NUMERICAL SIMULATIONS

We simulate numerically the transient flow in a pipeline subjected to a full guillotine break (see Section 6.1) and the transient gas dispersion downstream of the pipeline break location (see Section 6.3).

5.1. Parameters used in transient pipe flow problem

The length L and diameter D of the pipeline are chosen as 3×10^5 m and 0·7 m respectively. The initial temperature is chosen as 283 K inside and outside the pipeline. A linear pressure distribution is used with p_{max} and p_{min} located at the pipeline ends equal to 167 and 120 bar respectively. The corresponding initial density distribution is computed by iteration to satisfy the BWRSGES; see Section 2.2. A wet gas mixture is used; see Table II.

The initial turbulence level under the pipe flow operating conditions is characterized by the relative turbulence intensity 2%, the characteristic velocity 2 m s^{-1}, the turbulence length scale 0·3 m and a Reynolds number proportional to 10^7. The initial relative turbulence intensity is calculated on the basis of experiments carried out by Laufer,[10] the assumption of isotropic turbulence and the drag coefficient of Moody.[8] The turbulence length scale is estimated on the basis of Nikuradse's mixing length for pipe flow and a relation between the turbulence length scale and the mixing length.[20]

An expanding grid is used with the minimum control volume length located next to the pipeline break position. The minimum control volume length is 5 m and the grid expansion ratio is 1·1.

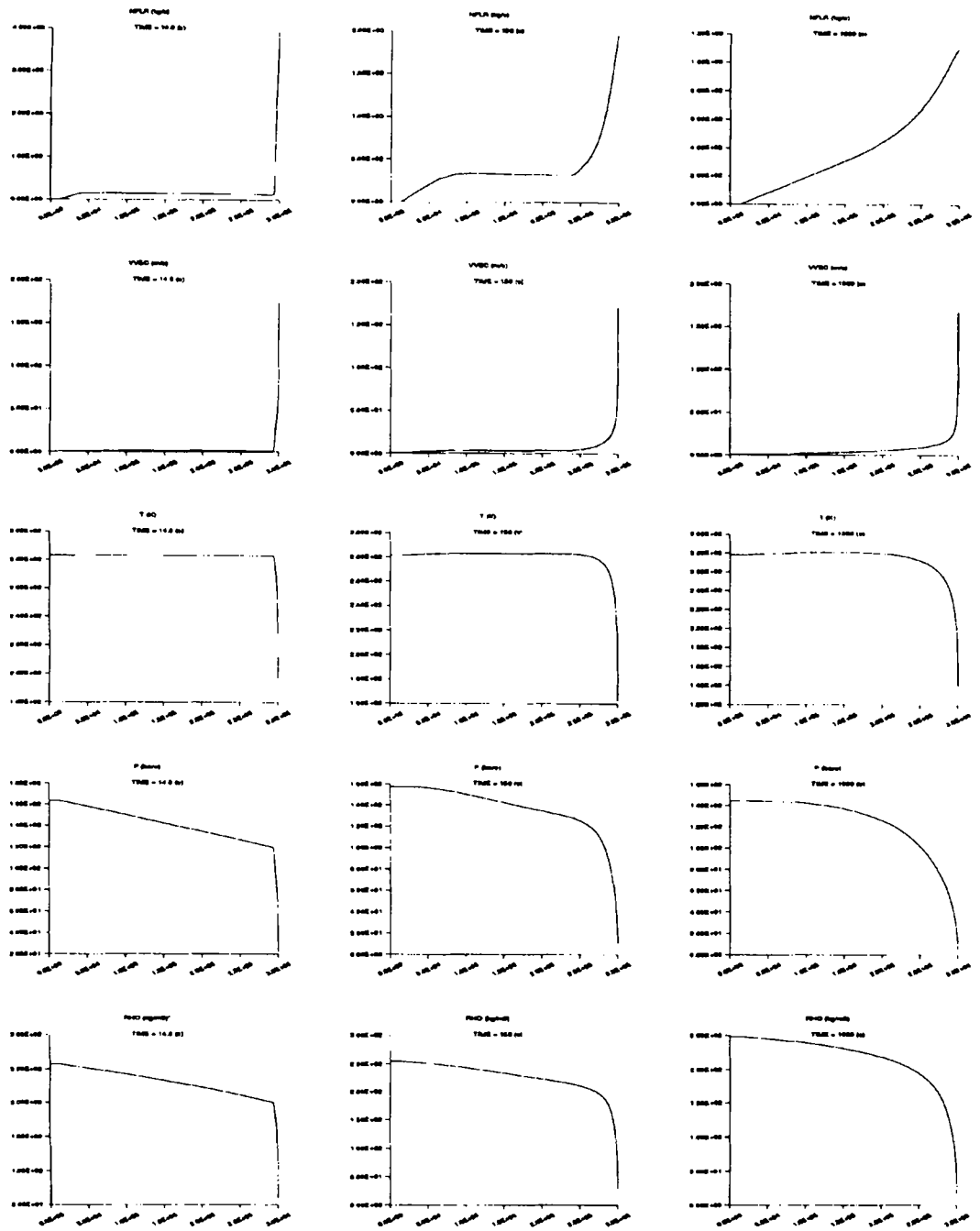

Figure 4. Flow rate, bulk velocity, temperature, pressure and density along pipeline for increasing time (left to right). The scale along the abscissa is metres

5.2. *Parameters used in transient dispersion simulation*

The computational domain for the dispersion problem is chosen to have the length 743 m, the width 512 m and the height 256 m. To reduce the storage requirement and the computation time, the gas leak is assumed to be located symmetrically with respect to a vertical plane cutting the pipeline axially. An expanding grid is used with a grid expansion of 1·1. The minimum control volume length is 5 m.

The jet is modelled on a subgrid level as a jet box. The equivalent nozzle area (see Section 3.4) is located 52·3 m downstream of the inflow boundary of the computational domain (see Figure 9). Ambient temperature and ambient pressure are 283 K and 1 bar respectively. The initial velocity, turbulence intensity and turbulent length scale are 0, 0·09 m s^{-1} and 0·005 m respectively.

5.3. *Graphical presentation*

The results from the numerical simulations are presented as graphical plots. We have recorded the flow rate, bulk velocity, temperature, pressure and density as functions of time at the break location and the same variables at three different time instants along the pipeline; see Figures 3 and 4 respectively.

The results from the transient dispersion simulation are reported as field plots of mixture fraction, absolute temperature and velocity. We have chosen six cut planes and 12 time instants to visualize the temporal and spatial variations in these fields.

The computed mixture fraction (see (43) for its definition) and the temperature are represented by filled contour plots in a grey tone-scale. The mixture fraction is plotted in Figures 5–7, where one and zero represent pure gas and air respectively.

The correspondence between the contour levels for the mixture fraction computed on a mass fraction basis and the contour levels for the molar fraction of the wet gas in the mixing stream is given in Table III. The temperature and velocity fields are shown in Figures 8 and 9–11 respectively.

6. DISCUSSION

6.1. *Transient pipe flow simulation*

The transient flow field in a long pipeline subjected to a full guillotine break at the lowest-pressure end has been studied using numerical simulations. Since the characteristic pipe flow speed (2 m s^{-1}) is very small compared with the sonic velocity, which occurs almost instantaneously after the break, the flow field is started from rest.

All the simulations carried out are characterized by a strong acceleration of the bulk flow from rest to choked flow. The chocked flow condition prevents pressure waves generated downstream of the pipeline break location from travelling upstream inside the pipeline. Only secondary effects from the flow field downstream of the pipeline break location can influence the flow field inside the pipeline. One such effect is the convective heating or cooling of the external side of the pipe wall carried out by the entrainment flow field; see Figures 9 and 10. This flow field results when the compressed fluid expands downstream of the pipeline break location. However, simulations carried out for both adiabatic and isothermal boundary conditions show that the heat flux from the pipe wall is negligible.

A simulation was also carried out for an alternative initial pressure distribution inside the pipeline using $p_{max} = 146$ bar and $p_{min} = 131$ bar. After approximately 1 s the simulated variables develop similarly with time as in the other case. The flow rate is approximately 10% higher and the temperature profile is close to identical.

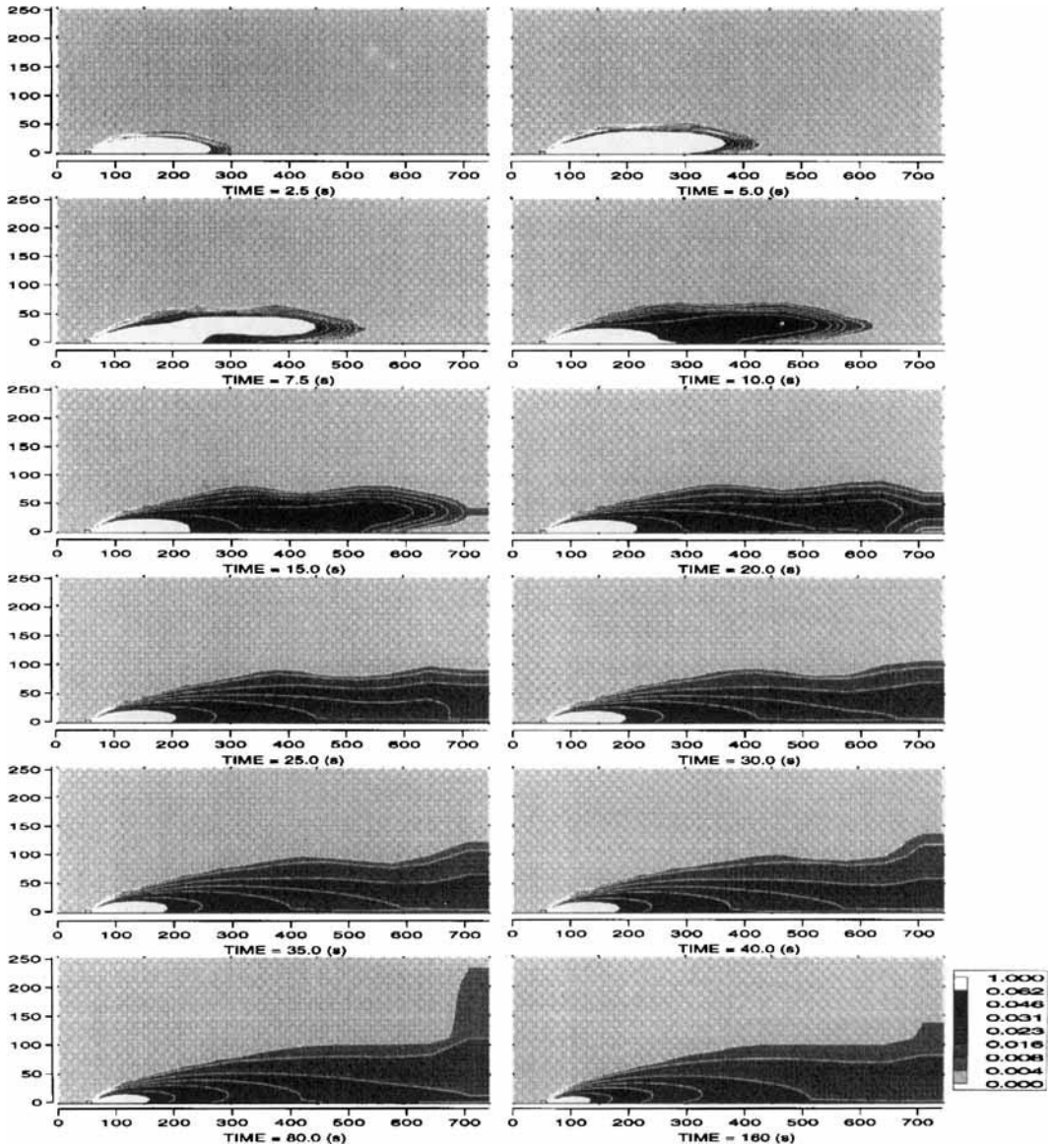

Figure 5. Mixture fraction f_{mix} at vertical cut in streamwise direction through jet box

When the break of the pipeline takes place, the bulk velocity drops by approximately 40% within 1 s and decelerates by about 5% within the next 1000 s; see Figure 3. The reduction in the bulk velocity after the gas flow is choked occurs because the gas density and the velocity of sound depend on the pressure and the temperature; see Tables IV and V.

As the gas discharges, the pressure inside the pipeline drops to maintain continuity of the mass flow through the choked flow condition at the pipeline break location. A continuous train of rarefaction waves forms inside the pipeline and travels upstream of the pipeline break location with the speed of sound relative to the flow field. The increased pressure gradient accelerates the flow field

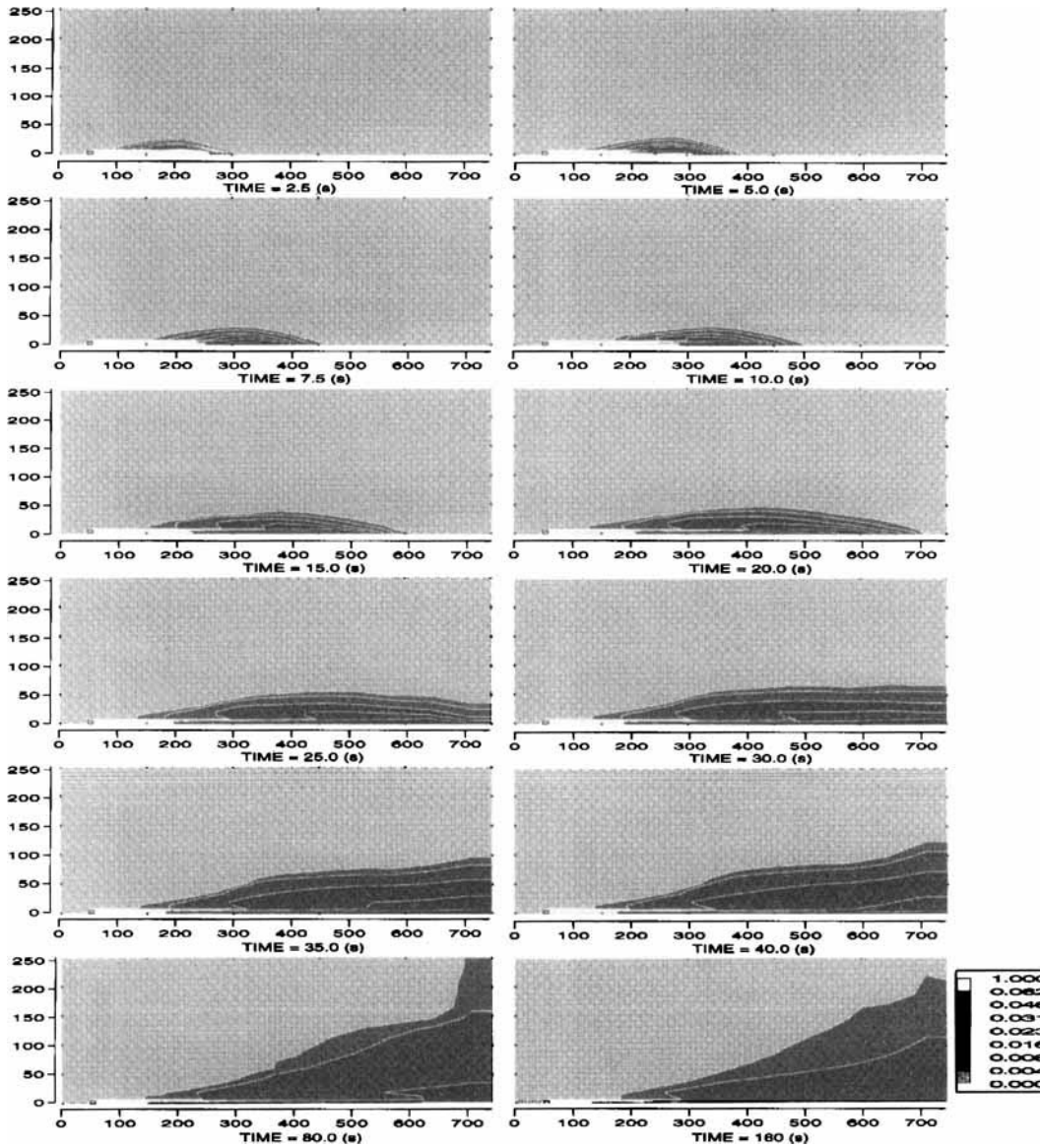

Figure 6. Mixture fraction f_{mix} at horizontal cut in streamwise direction through jet box

until viscous forces balance the pressure gradient. This process is continuous and changes over time the initial pressure distribution from linear to non-linear; see Figure 4.

Within 1 s the pressure and temperature at the pipeline break location drop by approximately 85 bar and 60 K respectively; see Figure 3. The temperature drop is a consequence of the expansion work done. However, part of the heat loss has been compensated by heat generation from viscous dissipation; Section 2.1. If the gas condensates, the heat of condensation will also help to minimizing the temperature drop; see the discussion in Section 6.2.

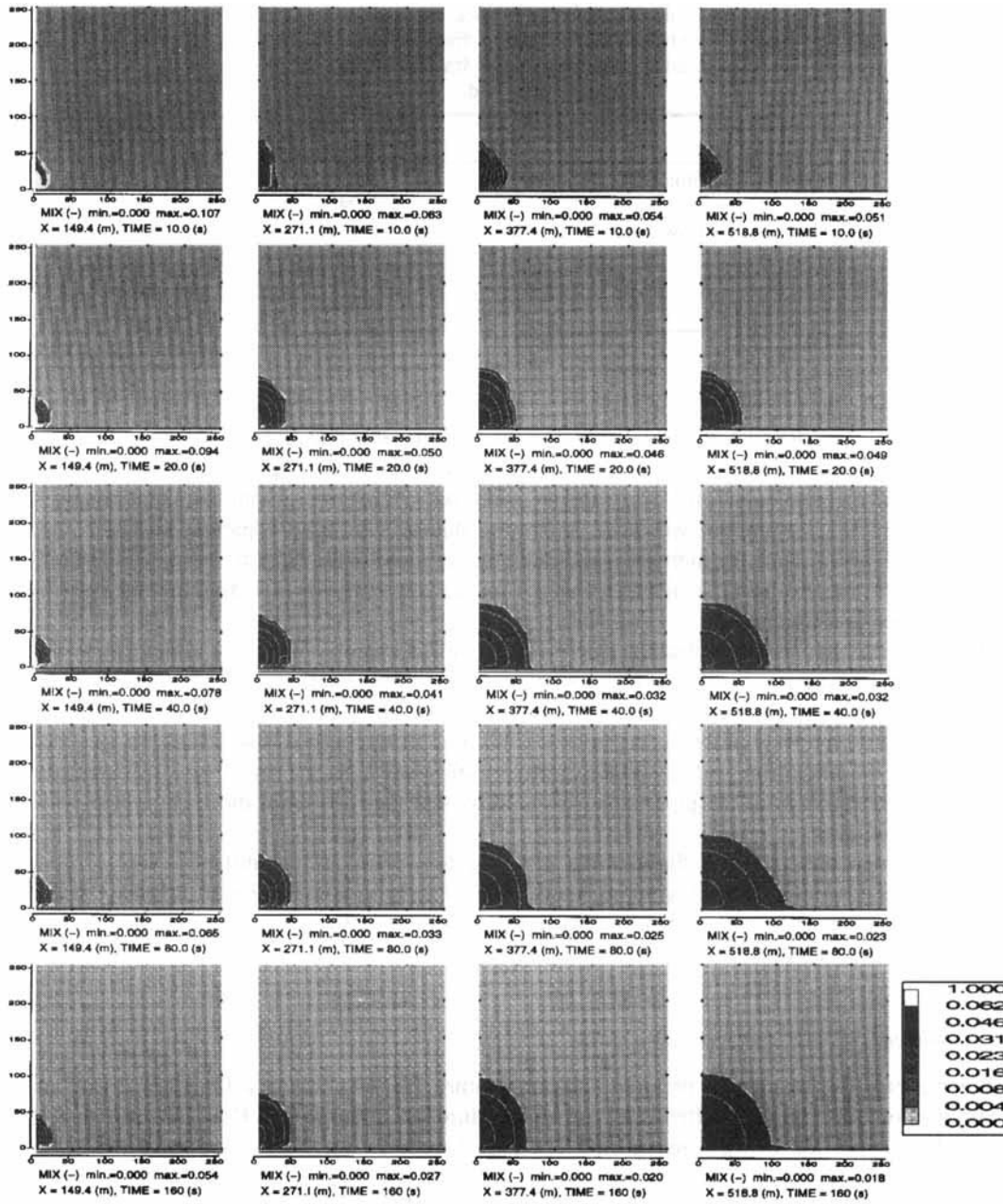

Figure 7. Mixture fraction f_{mix} for increasing time (top to bottom) at vertical cut planes normal to streamwise direction for increasing distance (left to right)

We have assumed that the pipeline is fully opened at the break location, so there is no geometrical effect included in the discharge coefficient, only the effect of viscosity. A measured velocity profile[8] is our basis. The discharge coefficient $C_D = 0{\cdot}82$ follows from the ratio between the bulk and the centreline velocity.

Table III. Correspondence between contour levels for mixture fraction and for total combustible molar fraction of mixture fluid

	X_M	f_{mix}
Stoich	0·08	0·062
	0·06	0·046
Lower f.l.	0·04	0·0305
	0·03	0·023
	0·02	0·016
	0·005	0·004

The use of the BWRSGES for computation of the velocity of sound and the density at the pipeline break location will also affect the maximum mass flow from the pipeline compared with that computed with an ideal equation of state and an isentropic gas relation. In our computations we have used a full enthalpy equation with heat generation due to viscous dissipation, so the computed temperature distribution in the high-pressure-gradient area close to the pipeline break location may be different from that of others. See also Section 2.1 for our approach for including the radial variation in the viscous dissipation term.

However, we have assumed that the internal pipe wall is smooth. This may affect the results. In contrast with the drag coefficient for a smooth pipe wall, the drag coefficient for flow in a fully rough pipe is independent of the Reynolds number but depends on the relative roughness height.[8]

The transient pipe flow problem was solved using two different grid resolutions. In the first and second cases the minimum grid size and expansion ratio were 5 m, 1·1 and 10 m, 1·3 respectively. The computed variables at the pipe outlet deviated by less than 1% from those computed with the lower grid resolution.

The time step used satisfies the Courant criterion $\Delta t_{n+1} = C_{ou} Dl_{\min} \min\{(c_s)^{-1}, (V_{\max})_n^{-1}\}$, were $DL_{\min}$ is the minimum control volume length and $(V_{\max})_n$ is the maximum velocity from the preceding time step. The transient pipe flow problem was solved for $C_{ou} \in [0{\cdot}2, 0{\cdot}4, 0{\cdot}6, 0{\cdot}8]$. The results from these simulations deviated by less than 1%.

6.2. Comments on retrograde condensation

When a pipeline breaks, the pressure and temperature fall very fast as a function of time at the break location; see Figure 3. After 100 s the temperature has fallen to 169 K and the pressure to 12 bar. Judging from the wet gas phase envelope (see Figure 1), the mass fraction of liquid in the corresponding equilibrium state is as high as 60% at the pipeline break location. Whether condensation will take place or not is therefore determined by the residence time of the gas in a state with high pressure and low temperature.

We have used an expanding grid where the shortest control volume has the pipeline break location as one of the control volume interfaces. An estimated residence time of the gas within this control volume is 0·03 s. From the experiments reported by Wegner[25] for condensation of supersaturated steam to water, it seems reasonable to conclude that the temperature gradient is too small and the residence time too long for the gas to leave the pipeline in a supersaturated state.

However, if condensation takes place, the temperature will increase as a consequence of the released heat of condensation. The actual mass fraction of liquid in the mixture will therefore be

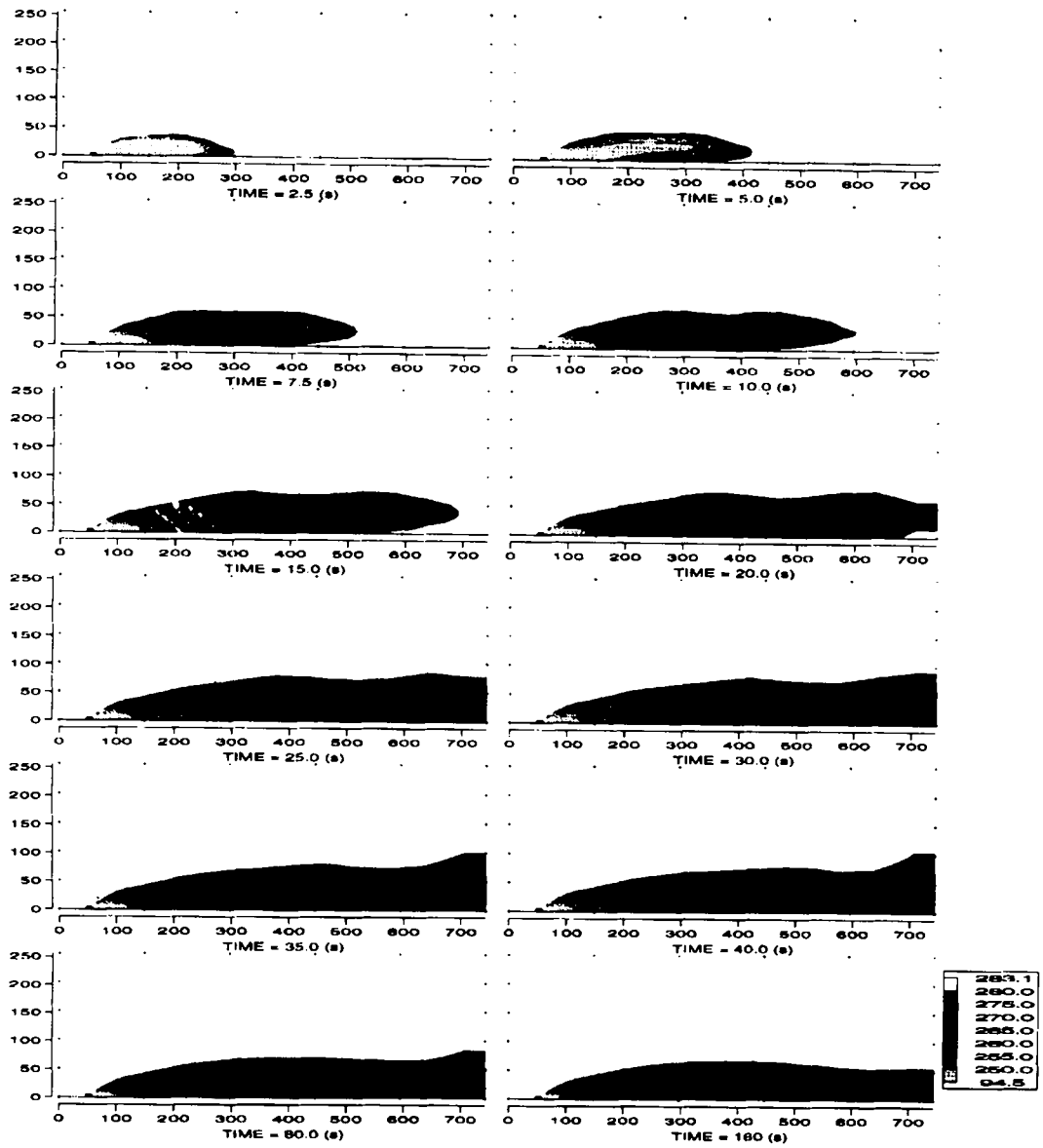

Figure 8. Absolute temperature at vertical cut in streamwise direction through jet box

smaller than the simulated 60%. The heat of condensation will act as a reversible factor against condensation within the pipeline (heat generation from viscous dissipation is already included in the one-dimensional simulation). A very rough estimate gives us 180 kJ kg^{-1} for the heat of condensation for the temperature inverval from 283 K to 169 K. From Table V we estimate the average specified heat capacity at constant pressure to be 2·6 kJ kg^{-1} K^{-1}. It follows that the temperature increase is approximately 70 K. This shows that if the gas condensates, the heat of condensation cannot be neglected when we want to calculate the mass fraction of liquid leaving the pipeline.

We have traced the computed state of the gas at the pipeline break location on the wet gas phase envelope as a function of time; see Figure 1. The curve for which the heat of condensation is included in the computations follows a path somewhere between the curve computed by us and that consisting of an isotherm from the end of the retrograde condensation area followed by a contour line for constant mass fraction of liquid.

If condensation takes place inside the pipeline, the inertia forces and the turbulent mixing are so strong close to the pipeline break location that the liquid phase is expected to be finely dispersed. Experimental values for dispersed water in steam by Karplus (see Reference 26) show that the velocity of sound will drop by about 20% and 30% for mass fractions of liquid of 30% and 50% respectively. This indicates that our flow rate, which is computed assuming that the fluid always stays in the gas phase, may be too high if condensation takes place inside the pipeline.

6.3. Transient dispersion simulation

A three-dimensional simulation of gas dispersion from a full guillotine break of a long pipeline is carried out. The break is at that end of the pipeline where the pressure is lowest.

The ratio between the pressure at the break point location and the ambient pressure is higher than the critical pressure ratio, so within a fraction of a second the flow is choked. As a consequence of the choking, the pressure at the break opening is higher than the ambient pressure; see Figure 3. It is well known that the gas expands over a distance proportional to D downstream of the pipeline break location and lowers the pressure to ambient pressure. The expansion accelerates the fluid from sonic to supersonic speed. The expansion area behaves as an equivalent nozzle of a supersonic turbulent jet. The phenomenon is known as underexpanded flow.

The supersonic turbulent jet acts as a pump where the shear forces entrain mass into the jet flow. The momentum flux, which is conserved except for loss because of viscous work on the ambient fluid, pushes the increased mass flux downstream. The entrainment sets up a secondary flow field which mixes air of ambient temperature with the very cold wet gas from the entrance of the turbulent jet.

The wet cold gas mixes within a short distance from the pipeline break location extensively with the warmer ambient air; see Figure 8. Far downstream of the jet entrance (at $x \approx 500$ m), only a small percentage of the mass of the mixing stream is wet gas; see Figure 5. Because of the inertia of the air, it takes time before the entrainment flow field is fully developed. As a consequence of this and the decay of the flow rate with time (see Figure 3), the lower flammability level for the wet gas ($f_{\text{mix}} = 0{\cdot}31$) reaches its most remote downstream position within the order of seconds; see Figure 5.

As the entrainment flow field becomes fully developed and the mass flow decreases, the lower flammability limit withdraws much closer to the pipeline break location. Qualitatively the distribution of contour levels for the mixture fraction looks right. Because of the wall friction, the dispersion of the gas is larger vertically than horizontally. Far downstream of the jet entrance (at $x = 519$m) the contour levels spread out more along the ground than above it as time passes; see Figure 7. This may be caused by the Coanda effect, i.e. the interaction between the jet and the boundary layer, and is not seen in the simulations carried out with the lowest grid resolution.

As a consequence of the expansion of the gas outside the pipeline break location, the temperature at the equivalent nozzle exit (the entrance of the jet) falls to 94·5 K during the 160 s shown in Figure 8. This is a lower value than the minimum temperature recorded at the pipeline break location during the 1000 s shown in Figure 3. This temperature is below the condensation temperature of our gas composition. Our wet gas is therefore supersaturated as it leaves the equivalent nozzle exit. This is a consequence of our assumption of treating the gas as a single phase.

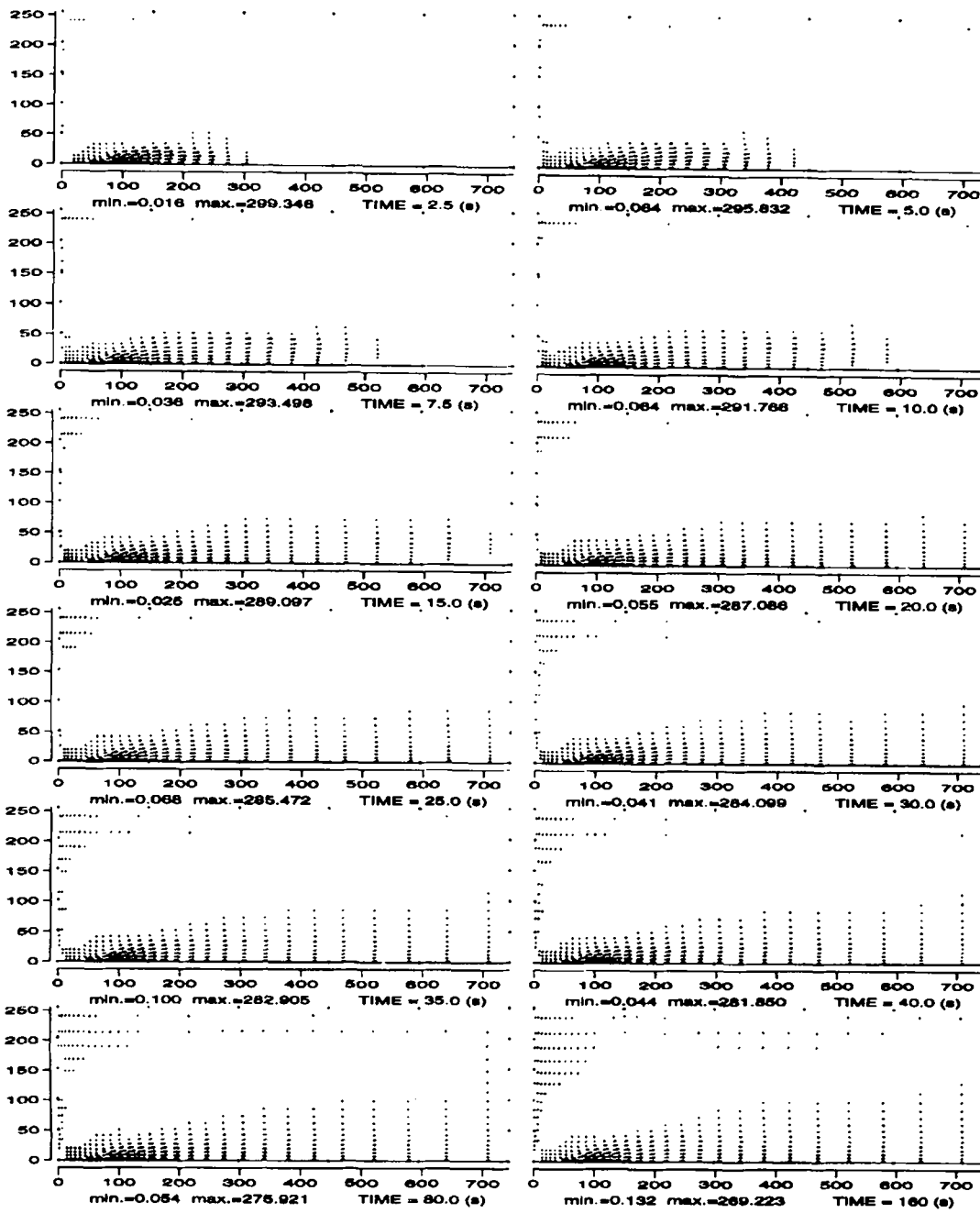

Figure 9. Velocity plots at vertical cut in streamwise direction through jet box

Table IV. Computed and experimental thermodynamic properties of nitrogen

T(K)	P(bar)	ρ(kg m^{-3})		c_p(J kg^{-1} K^{-1})		h(J kg^{-1})		c(m s^{-1})	
		comp.	exp.	comp.	exp.	comp.	exp.	comp.	exp.
200	1	1·6884	1·6883	1043	1043	207064	207000	288·0	288·1
200	40	73·899	73·153	1249	1251	188409	187800	281·7	286·1
200	100	202·65	199·24	1658	1640	158976	159000	308·0	316·7
200	200	374·14	371·16	1848	1798	128958	131000	434·0	
300	1	1·1236	1·1233	1040	1041	311179	311120	353·1	353·1
300	40	45·549	45·086	1096	1102	303161	303000	356·9	361·2
300	100	113·19	111·73	1183	1189	292492	292000	377·8	380·4
300	200	211·94	212·72	1297	1294	280467	279300	440·5	
400	1	0·84228	0·84246	1045	1045	415374	415400	407·4	407·4
400	40	33·603	33·278	1070	1076	411089	411600	413·6	417·8
400	100	82·341	81·169	1107	1119	406127	406800	433·0	437·4
400	200	154·63	154·18	1160	1175	401928	401500	482·7	

As we commented in Section 6.2, we expect that condensation will take place within the pipeline because of the long residence time of the gas in a state of high pressure and low temperature. However, should this not be the case, the condensation will start at the exit of the equivalent nozzle and be followed by an increase in temperature because of the released heat of condensation. This is illustrated by the rough estimate of the temperature increase given in Section 6.2, which shows that the heat of condensation should not be neglected when we estimate the mass fraction of condensated liquid. As already mentioned, as the wet cold gas moves downstream it becomes extensively mixed with the warmer ambient air and the gas mixture reaches a temperature where the condensated gas will evaporate. This requires heat, so, provided that there is no rain-out, the temperature will recover to that of a single-phase gas mixture some distance downstream of the equivalent nozzle exit. Figure 8 shows that it is only at the equivalent nozzle exit that the temperature is as low as 94·5 K. The minimum temperature elsewhere is 250 K.

We have plotted the velocity field in Figures 9–11. It should be noted that the velocity vectors shown are interpolated values at the centres of the control volumes. This has the consequence that the velocity at the jet box centre, which is the maximum velocity in the field, is only half the jet box exit value. Basically the velocity plots show that the momentum flux from the supersonic turbulent jet is the driving force of the flow field. The development of the large recirculation zone representing the entrainment velocity field is shown at a vertical and a horizontal cut plane through the jet in Figures 9 and 10 respectively. These figures also show that there are oscillations at the inlet boundary upstream of the jet box. These oscillations may be a consequence of the transient computations.

The dispersion problem was solved using two different grid resolutions. In the first and second cases the minimum grid size and expansion ratio were 5 m, 1·1 and 10 m, 1·3 respectively. The lower flammability level of the gas mixture (0·031) was carried furthest downstream when the highest grid resolution was used, approximately 600 m compared with 500 m. The timing of these events was also different, approximately 15 s compared with 10 s.

The stoichiometric limit (0·062) was carried approximately 440 m downstream when the highest grid resolution was used (see Figure 5), while the code could not follow this concentration level after the first 2·5 s of simulated time when the lowest grid resolution was used. This seems reasonable, since all scalar variables computed at a particular node point are averaged values with the control

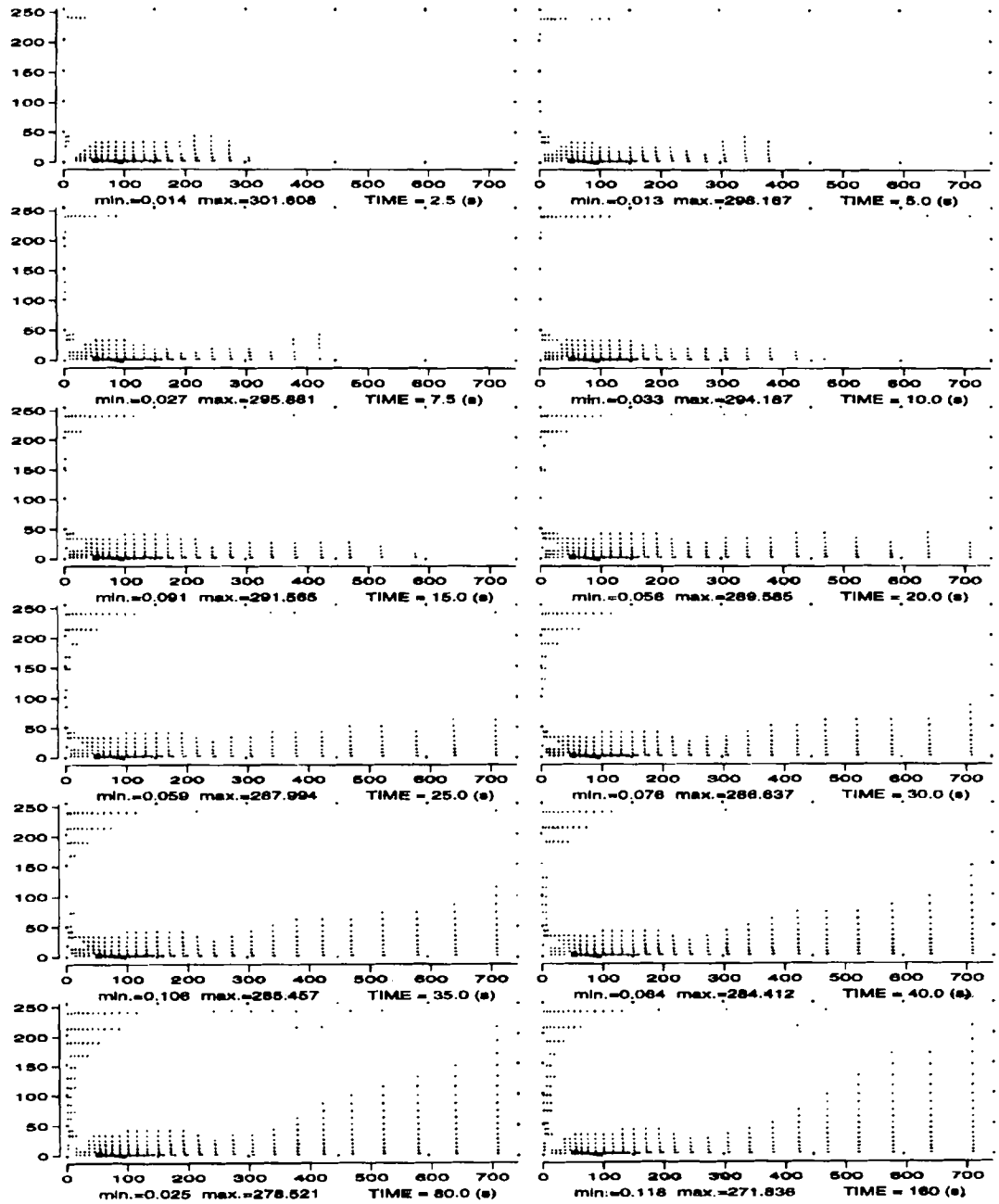

Figure 10. Velocity plots at horizontal cut in streamwise direction through the jet box

Table V. Computed and experimental thermodynamic properties of wet gas

T(K)	P(bar)	ρ(kg m^{-3})		c_p(J kg^{-1} K^{-1})		h(J kg^{-1})		c(m s^{-1})		$\gamma = c_p/c_v$	
		comp.	exp.	comp.	exp.	comp.	exp.	comp.	exp.	comp.	exp.
200	1·0132	1·3500	1·3500	1763	1769	−2975790	−2976000	310·1	310·3	1·29489	1·29502
200	50										
200	100										
200	200										
300	1·0132	0·89000	0·89000	1989	1994	−2789500	−2789000	375·2	375·1	1·24113	1·24082
300	50	53·100	53·100	2610	2615	−2857970	−2858000	340·1	345·0	1·49634	1·49514
300	100	130·76	130·73	3612	3648	−2940640	−2941000	343·4	344·1	1·98153	1·99562
300	200	254·91	254·85	3502	3508	−3030190	−3030000	518·4	497·0	2·06965	2·06718
373·15	1·0132	0·7200	0·7100	2233	2244	−2635350	−2635000	413·4	418·6	1·20744	1·20580
373·15	50	38·09	38·09	2477	2489	−2675440	−2675000	398·5	408·3	1·29912	1·29770
373·15	100	81·09	81·07	2777	2791	−2717160	−2716000	401·1	410·4	1·42467	1·42325
373·15	200	164·4	164·4	3172	3189	−2783780	−2783000	472·8	464·1	1·61506	1·61468

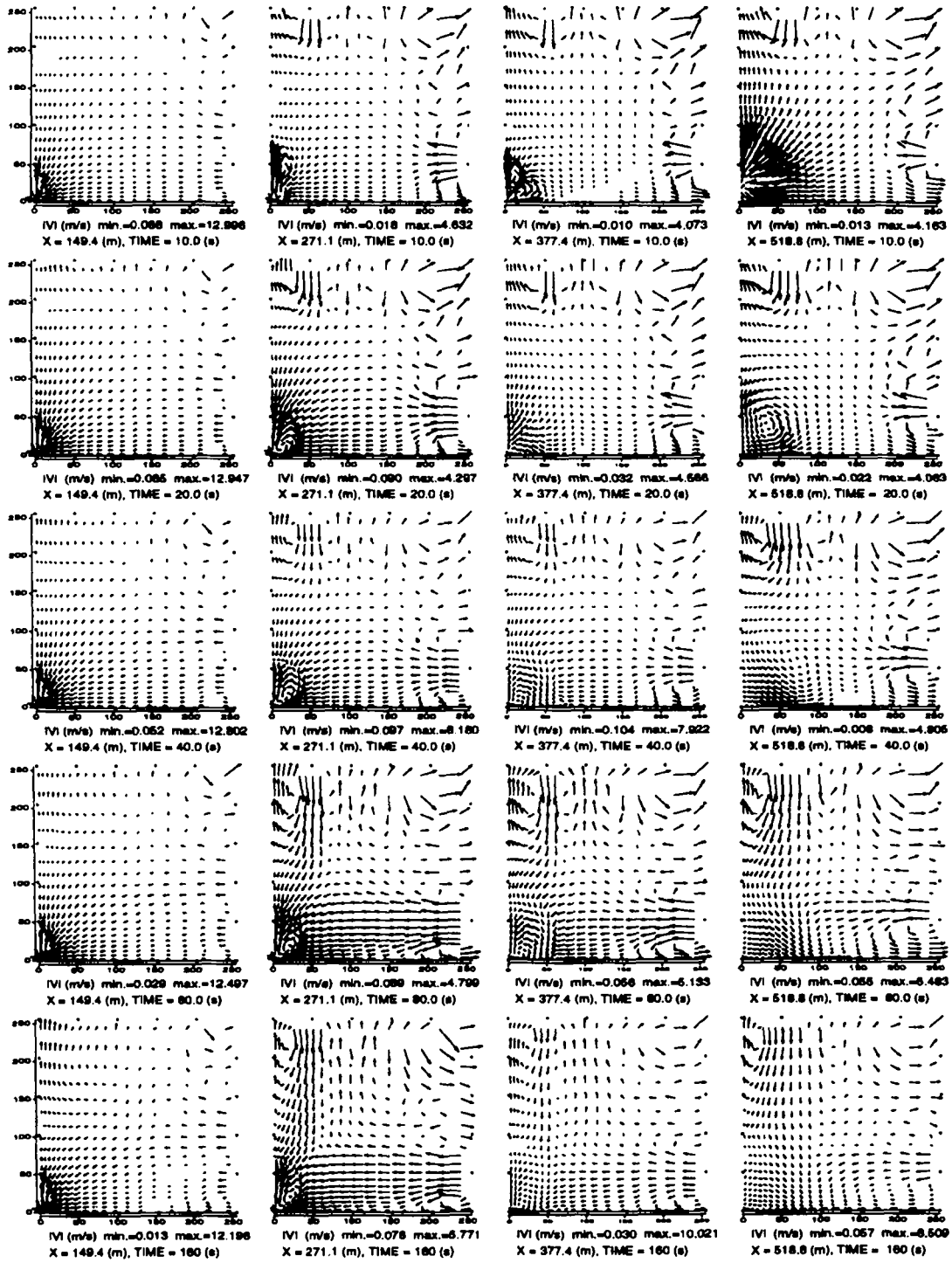

Figure 11. Velocity plots for increasing time (top to bottom) at vertical cut planes normal to streamwise direction for increasing distance (left to right)

volume surrounding the node point. The more details we want, the higher is the grid resolution required.

Also the tendency of the jet to stay along the ground was more pronounced for the higher grid resolution. This Coanda effect, i.e. the interaction between the jet and the boundary layer near the ground, is in principle taken care of by the two-layer wall function procedure implemented for the three-dimensional dispersion problem.

However, the qualitative behaviour of the flow field did not change as a consequence of the increased grid resolution. The lower flamability limit of the gas–air mixture reaches its most remote downstream position relatively early in the simulation and withdraws closer to the pipeline break location as time passes by. Even the highest grid resolution is still relatively coarse for much of the dispersion area shown in the figures. We can therefore only expect the results to be qualitatively right.

Also for the dispersion problem both adiabatic and isothermal boundary conditions were used. The effect of considering the ground to be isothermal did not give significant change in the concentration field compared with assuming the ground to be isolated.

The effect of buoyancy on turbulence generation or destruction was also checked and shown to be insignificant with respect to changing the velocity or concentration field. However, as can be seen from Figures 5 and 8, buoyancy is affecting the flow and concentration fields through the momentum equation. The cold heavy flow which is lifted up because of the development of a boundary layer separation around the 400 m mark along the x-axis (see Figure 9 from TIME = 5·0 s to TIME = 10·0 s) tips down again for concentration level 0·046 at TIME = 15·0 s and for level 0·031 at TIME = 20·0 s; see Figure 5.

The Courant number used in these simulations was unity. The initial phase of the simulation (10 s) was carried out also using the value 0·5 without significant change in any field variables.

To get a feeling for the accuracy of the simulations, we have compared the inverse normalized maximum velocity $(U_m/U_e)^{-1}$ and inverse maximum concentration level as a function of normalized displacement $(X - a)/D_e$ and X/D_e respectively with data from an underexpanded steady vertical jet,[3,27] were a is a correction distance for pseudosource location and U_e and D_e are the equivalent velocity and diameter respectively. Birch *et al.*[3,27] showed that using this scaling with a and D_e being functions of the ration between reservoir and ambient pressure, similarity solutions exist for the axial values.

In this comparison we have used the simulated data as if they were actual measured data, taking the pressure from Figure 3 at the time instances 10, 20, 40, 80 and 160 s. The corresponding reservoir pressures at the time instances chosen for comparison are calculated using the same isentropic flow relation as that of Birch *et al.*[3] covering a reservoir pressure range from 51 to 25 bar.

Since our jet has the character of a wall jet, we have used maximum values (in a cut plane normal to the flow direction) of the velocity and concentration level instead of the axial values. The results are shown in Figures 12 and 13.

As can be seen from Figure 12, the maximum normalized velocity approaches a similarity solution (all data approximately in one line) as time increases and the flow field changes slower as a function of time, getting closer to the character of a steady jet. However, the slope has a lower value than that of Birch *et al.*[3] This seems reasonable, since the maximum velocity of the wall jet will be higher than the axial velocity of the axisymmetrical jet, which is a consequence of no entrainment of mass into the jet from the wall-bounded side.

The concentration level does not approach the same similarity solution as that of Birch *et al.*[27] However, the order of magnitude is correct, approximately 50% of the experimental values. Also the concentration level decreases as the time increases, indicating that the grid resolution is too low to follow the concentration level as the gas is carried far downstream of the pipeline break location.

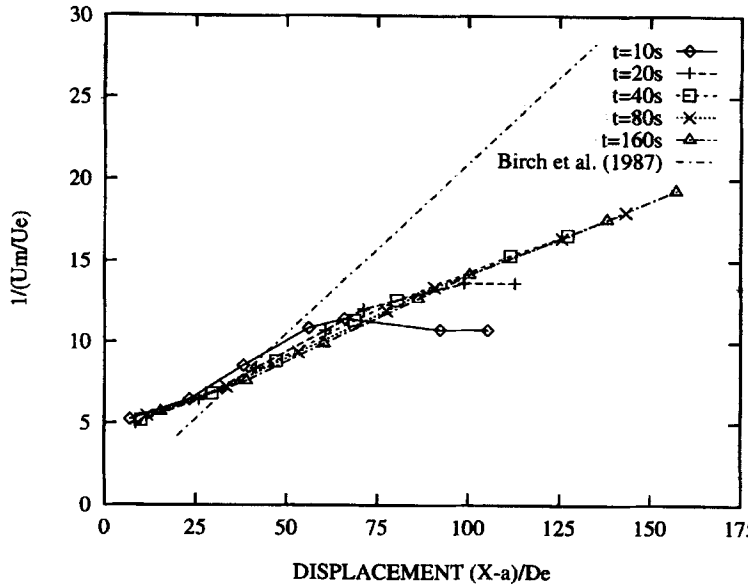

Figure 12. Normalized inverse maximum velocity as a function of normalized horizontal displacement compared with data from an underexpanded steady vertical jet

We conclude that a comparison with transient experiments would have been better; however, that would require that a similarity solution exists for the transient flow problem to avoid carrying out a full-scale experiment.

7. CONCLUSIONS

The computed mass flow from the pipeline break location depends on the initial exit pressure but is relatively independent of the initial pressure gradient inside the pipeline as long as the initial pressure gradient is high enough to support the choked flow condition.

The computed mass flow of gas from the pipeline break location becomes supersaturated less than 1 s after the break of the pipeline. In the corresponding equilibrium state, approximately 50% of the mass is liquid condensate. However, the heat of condensation is so high that it is necessary to include it to compute accurately the mass fraction of condensate.

Experiments carried out for dispersed water in steam by Karplus (see Reference 26) show that the velocity of sound will drop by about 20% and 30% for liquid mass fractions of 30% and 50% respectively. This indicates that the mass flow computed by us will be too high if condensation takes place inside the pipeline and disperses evenly.

From a qualitative point of view the computed dispersion of gas seems right, taking into consideration that the gas is simulated as being supersaturated at the exit of the equivalent nozzle.

The temperature recovers within a short distance downstream of the equivalent nozzle exit and the gas ceases to be supersaturated. This is a consequence of the turbulent mixing of the gas with the warmer ambient air.

Buoyancy affects the dispersion of the mixed gas; however buoyancy-generated production or destruction of turbulence did not have a significant effect on the concentration or velocity field.

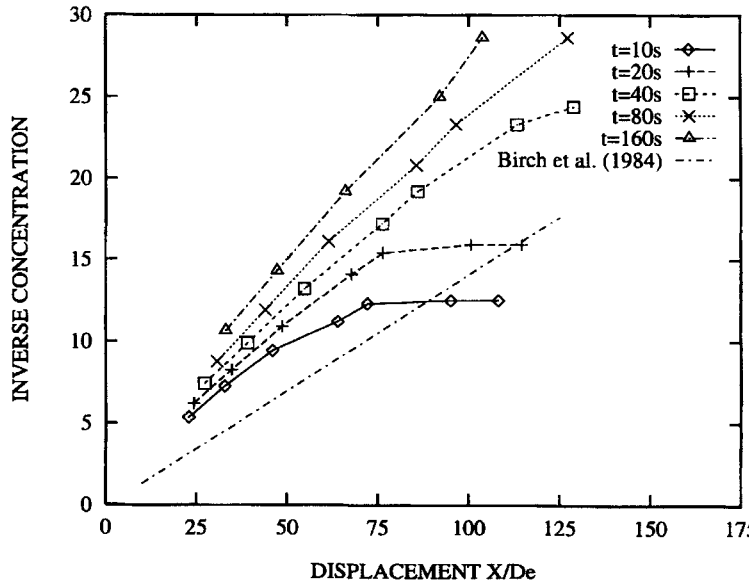

Figure 13. Maximum concentration (molar fraction) as a function of normalized horizontal displacement compared with data from an underexpanded steady vertical jet

Owing to the inertia of the ambient air, it takes time to develop the entrainment flow field. A large three-dimensional recirculation zone develops gradually. It transports air from regions far away from the jet axis and far downstream of the equivalent nozzle exit and injects it closer to the jet entrance, where the air is entrained into the jet.

The flammability limit reaches its most remote downstream position before the secondary entrainment velocity field is fully developed. Owing to increased turbulence and decreasing mass flow with time, the lower flammability limit withdraws fast towards the entrance of the jet (the equivalent nozzle exit).

Simulations with one relatively high and one low grid resolution give qualitatively the same results. However, the position of the lower flammability limit as a function of time and space reaches further downstream when the higher grid resolution is used.

There was not significant difference in the flow rate from the pipe using either isothermal or adiabatic boundary conditions on the pipe wall. Neither was there any significant difference in the concentration fields using either isothermal or adiabatic boundary conditions on the ground for the dispersion problem.

Experimental data for transient underexpanded flow were not available in the literature. However, a comparison with a steady underexpanded axisymmetric jet for varying reservoir pressure (51–25 bar) indicates that the simulated data are correct within an order of magnitude.

ACKNOWLEDGEMENTS

This work has been financially supported by Statoil. The one-dimensional code used for the pipeline flow problem was designed for this project uniquely. The computer programme design used in the three-dimensional dispersion simulation is an extension of the FLACS-89 code to handle real gases. The original FLACS code was developed at CMR on the basis of a general-purpose incompressible fluid and heat transfer computer code by S. V. Patankar. The calculation of the static data and the

velocity of sound used for comparison were carried out by Ben Velde, Statoil, using Son-flow 86 and a thermodynamic package available at Statoil. The author acknowledge Professor Dag Bjerketved, Telemark Institute of Technology, for support and discussions and Idar Storvik CMR for help with the graphical presentation.

REFERENCES

1. H. Reichardt, 'Die grundlagen des turbulenten Wärmeyberganges', Ach. Ges. Wärmetech., **6–7**, 129–143 (1951).
2. B. S. Petukov, *Numerical Heat Transfer and Fluid Flow*, McGraw-Hill, New York, 1980.
3. A. D. Birch, D. J. Hughes and F. Swaffield, 'Velocity decay of high pressure jets', *Combust. Sci. Technol.*, **52**, 161–171 (1987).
4. D. B. Spalding, *Combustion and Mass Transfer*, Pergamon, Oxford, 1979.
5. C. C. Chieng and B. E. Launder, 'On the calculation of turbulent heat transport downstream from an abrupt pipe expansion', *Numer. Heat Transfer*, **3**, 189–207 (1980).
6. W. Hossain and W. Rodi 'A turbulence model for buoyant flows and its application to vertical buoyant jets', in W. Rodi (ed.), *Turbulent Buoyant Jets and Plumes*, Pergamon, New York, 1982.
7. A. Favre, 'Equations des gaz turbulents compressibles', *J. Méc.*, **4**, 361–390 (1965).
8. W. M. Kays and M. E. Crawford, *Convective Heat and Mass Transfer*, 2nd edn., McGraw-Hill, New York, 1980.
9. W. H. McAdams, *Heat Transmission*, 3rd edn., McGraw-Hill, New York, 1954.
10. J. Laufer, 'The structure of turbulence in fully developed pipe flow', *National Advisory Committee for Aeronautics, Rep. 1174*, 1953.
11. R. B. Bird, W. E. Stewart and E. N. Lightfoot, *Transport Phenomena*, Wiley, Chichester, 1960.
12. K. E. Starling, *Fluid Thermodynamic Properties for Light Petroleum Systems*, Gulf, 1973.
13. E. Lang and T. K. Fanneløp, 'Efficient compuation of the pipeline break problem', *Proc. ASME Winter Ann. Meet.*, ASME, New York, 1987.
14. F. G. Blottner, 'Influence of boundary approximation and conditions on finite-difference solutions', *J. Comput. Phys.*, **48**, 246–269 (1982).
15. A. Melvin, *Natural Gas: Basic Science and Technology*, British Gas/ Adam Hilger, Bristol, 1988.
16. J. F. Douglas, J. M. Gasiorek and J. A. Swaffield, *Fluid Mechanics*, Pitman, New York, 1979.
17. P. A. Thompson, *Compressible-Fluid Dynamics*, McGraw-Hill, New York, 1972.
18. B. E. Launder and D. B. Spalding, 'The numerical computation of turbulent flows, *Comput. Methods Appl. Mech. Eng.*, **3**, 269–289 (1974).
19. I. Ø. Sand and J. R. Bakke, 'Wall-function boundary conditions in the solution of the Navier–Stokes and the energy equations', *Chr. Michelsen Institute, Rep. CMI- 25110-3*, 1989.
20. B. E. Launder and D. B. Spalding, *Lectures in Mathematical Models of Turbulence*, Academic, New York, 1972.
21. S. V. Patankar, *Numerical Heat Transfer and Fluid Flow*, McGraw-Hill, New York, 1980.
22. S. V. Patankar and D. B. Spalding, 'A calculation procedure for heat, mass and momentum transfer in three-dimensional parabolic flows', *Int. J. Heat Mass Transfer*, **15**, 1787–1806 (1972).
23. A. J. Chorin, 'Numerical solutions of Navier–Stokes equations', *Math. Comput.*, **22**, 745–762 (1968).
24. B. H. Hjertager, 'Computer simulation of turbulent reactive gas dynamics', *Model. Ident. Control*, **5**, 211–236.
25. P. P. Wegner, *Nonequilibrium Flows, Part I*, Marcel Dekker, New York, 1969.
26. G. B. Wallis, *One-Dimensional Two-Phase Flow*, McGraw-Hill, New York, 1969
27. A. D. Birch, D. R. Brown, M. G. Dodson and F. Swaffield, 'The structure and concentration decay of high pressure jets of natural gas', *Combust. Sci. Technol.*, **36**, 249–261 (1984).
28. W. C. Reynolds and H. C. Perkins, *Engineering Thermodynamics*, 2nd edn., McGraw-Hill, New York, 1977.
29. I. Ø. Sand, 'Massive release of gas from high pressure pipelines using turbulence models and the BWRS generalized equation of state', *Chr. Michelsen Institute, Rep. CMI-90-F25005*, 1990.
30. K. Sjøen, 'Dense phase gas transport in Statpipe', *Proc. Conf. on Multiphase Flow-Technology and Consequences for Field Development*, Norwegian Petroleum Society, Stavanger, 1987.
31. N. B. Vargaftik, *Handbook of Physical Properties of Liquids and Gases*, 2nd edn., Hemisphere, New York, 1983.